Multi-electron secondary emission from solid surface bombarded by fast atomic particles

V. B. Leonas

Institute of Problems in Mechanics, Academy of Sciences of the USSR, Moscow
(Submitted July 9, 1990; resubmitted November 21, 1990)
Usp. Fiz. Nauk **161**, 73–100 (April 1991)

This article reviews the most recent experimental approaches to the study of, and the results of investigations of multi-electron secondary emission resulting from the bombardment of the surface of a solid by atomic particles with energies of $1-10^3$ keV. The results of measurements of the differential characteristics of secondary electron emission (emission statistics, energy and angular distributions) are discussed. Theoretical approaches to a quantitative description of the principal characteristics of multi-electron secondary emission are considered, and the results of a Monte Carlo modeling, reproducing the principal observed MUSE effects are discussed.

1. INTRODUCTION

Secondary electron emission is one of the fundamental processes involved in the interaction of a plasma with a solid. The phenomenon of secondary electron emission from the surface of a solid being bombarded by high-energy particles (atoms or ions) has been known for a long time, the first publication[1] having appeared in the last century. A very large amount of experimental data has been gathered up to the present time,[2,3] and serves as the basis for the phenomenological and semiempirical theories of the phenomenon (see appropriate citations in Ref. 3).

It must be pointed out that the recognition of the key role of surface cleanliness and the mastery of ultrahigh vacuum techniques have led in many cases to a discrediting of old data and the implementation of new experimental programs. Therefore, the experimental information resulting from secondary electron emission studies during the past 10–15 years has obvious priority and reliability.

Traditional objects of secondary emission studies are the yield γ—the average number of secondary electrons per bombarding particle and the energy spectrum of the secondary yield $d\gamma/dE_e$. These measurements have been made both on massive as well as thin (transparent to the primary particles) targets. Recently, in addition to the above-mentioned integral characteristics, considerable attention has been paid to the differential characteristics—secondary yield statistics (distribution in terms of the number of secondary electrons leaving the surface), symmetry of the forward/backward yield (with respect to the direction of the bombarding beam), angular and energy distributions of the secondary emission. Figure 1 illustrates qualitatively the experimental possibilities for the two types of targets. In speaking of secondary electron emission we have in mind a discussion of the so-called kinetic emission, caused by a bombardment with heavy atomic particles. We will not consider potential emission. We will only mention the fact that the level of today's experimental techniques[4] makes it possible to regard investigations of potential emission, caused by slow multiply charged ions, as being extremely promising in the development of a method of spectroscopy of the electron states in a solid. The good prospect of success here comes from the development of plasma sources of multiply charged ions,[5] the almost routine capability of obtaining atomically clean surfaces, and the development of appropriate novel methods[6] for investigations with slow ions such that the contribution of kinetic emission is completely precluded.

The conclusions that have been reached from available data of the investigation of kinetic secondary electron emission are reflected in the interpretation of an emission event as the result of a process consisting of three successive stages:

A. Primary ionization by a high-energy particle passing through the material (secondary ionization processes by high-energy internal electrons and recoil atoms are also possible).

B. The migration of the resulting internal electrons to the material-vacuum interface.

C. Escape of emission electrons into vacuum after surmounting the surface potential barrier.

These stages are found in all known theories of secondary emission, and such a formalization of the process reflects the following key observational data:

1. The emitted secondary electrons are produced primarily in a thin near-surface layer of the material, within the characteristic escape depth λ_e.

2. The angular distribution of the escaping secondary electrons for noncrystalline targets is close to a cosine distribution.

3. The shape of the secondary electron energy distribution is not very sensitive to changes in the energy or incidence angle of the primary particles.

4. The maximum secondary yield is reached at energies < 1 keV for bombardment by electrons and at energies $< 10^2$ keV for protons (for heavier particles the maximum is shifted in proportion to m_A/m_H).

5. The secondary yield increases with the incidence angle θ (see Fig. 1).

6. The secondary yield for nonconducting materials generally exceeds the yield for metals.

All of these conclusions are arrived at on the basis of measurements of the integral (total yield, energy spectrum of electrons averaged over angles, angular distribution of escaping secondary electrons averaged over energies), leaving considerable arbitrariness for understanding the actual physical mechanisms underlying the secondary electron emission phenomenon.

It appears that differential measurements that have been incorporated into programs in recent years—measurements of the emission statistics and twofold differential

 0038-5670/91/040317-14$01.00

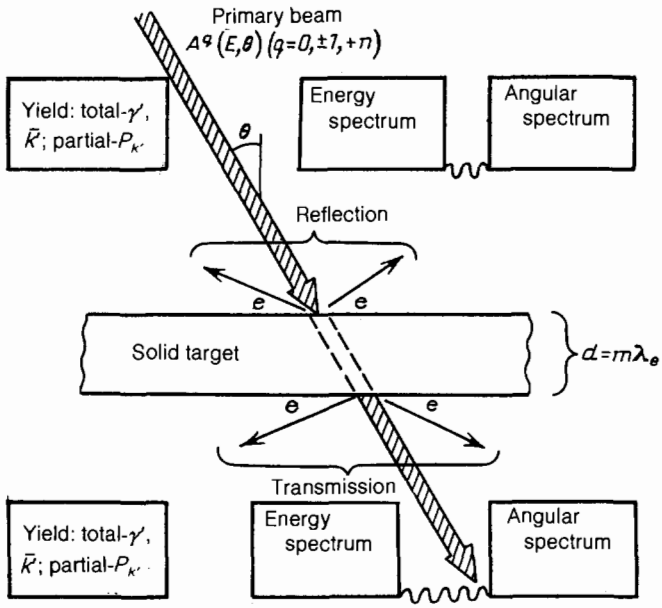

FIG. 1. Schematic representation of the characteristics and configuration of the experiment as well as the measured quantities for a study of secondary electron emission. The target thickness must be expressed in relative units $m = d/\lambda_e$ rather than in absolute units. The wavy lines represent possibilities for carrying out measurements simultaneously or in coincidence.

yields (with respect to angle and energy)—will make it possible to "narrow the tolerances" drastically on the admissible mechanisms incorporated in the theories and to bring us closer to a quantitative understanding of the phenomenon of multielectron secondary emission. With the term multielectron we are emphasizing that the total yield γ that is usually measured is the statistical mean of events of different multiplicity in the individual emission events.

This review paper is devoted to these directions of study of recent years. The principal factors of the above-mentioned changeover in experimental techniques are the elimination of current measurements in favor of discrete counting, the use of beams of atoms and variously charged ions, and thin targets (or foils). This provides for both a control of the interaction energy as well as controllable distributions of the charge states of the high-energy particles. A typical curve showing the variation of the charge state is illustrated in Fig. 2 for H^+ and H^0 beams ($E = 6$ keV) passing through a gold target. The close-to-asymptotic value of $\bar{q} = 0.33$ for the ion fraction is reached after traversing ~ 100 Å; for thinner targets we see large differences in the ion fractions in the H^+ and H^0 beams traversing a path length of $x < 10^2$ Å. These variations in the case of thin targets provide a means of assessing the asymmetry of the forward/backward yields, caused by the charge state of the atomic particle passing through the target.

One aspect of the attempts undertaken to analyze secondary electron emission data theoretically is the fact that the secondary electrons span an energy range of four orders of magnitude (1–10^4 keV). Over such a range, encompassing both slow and fast (on the Bohr velocity scale) collisions, we can scarcely assume that either the mechanism of generation or the energy and angular spectra of the internal secondary electrons remain constant. The need to span such a large range has prompted attempts to scale secondary emission effects to the quantity $(dE/dx)_e$—losses due to the so-called electron-induced stopping in the target material. Using the stopping power, which can be measured and calculated, one can close, as it were, the question of the actual collision mechanisms of ionization. However, the attractiveness of a description on this one basis must not hide the fact that the description is purely phenomenological, and the corresponding theory will have minimum predictive power. Moreover, it will be seen below that of the total loss in the slowing of a fast particle passing through the target, only 15–20% is actually used in the generation of internal electrons; this relation will limit the accuracy of any quantitative predictions based on the quantity $(dE/dx)_e$.

Figure 3 shows a qualitative picture of the passage of a high-energy atomic particle through a thin target; with its aid we can discuss the principal collision processes associated with secondary electron emission.

As seen from Fig. 3, a heavy particle, after traversing a path x_k ($k = 1,2,3$) determined by the characteristic ionization mean free path λ_i ($x_k = -\lambda_i \ln \xi$, where ξ is a random number in the interval from 0 to 1), produces an internal secondary electron e_k. The mean-free-path λ_i is determined by the effective ionization cross section Q_i and by the density n of the target material ($\lambda_i = (Q_i \cdot n)^{-1}$). The escape of the internal secondary electrons is usually assumed to be isotropic. A model of isotropic escape in the center-of-mass system of the colliding atoms would be more exact. Then a consideration of the motion of the center-of-mass gives rise

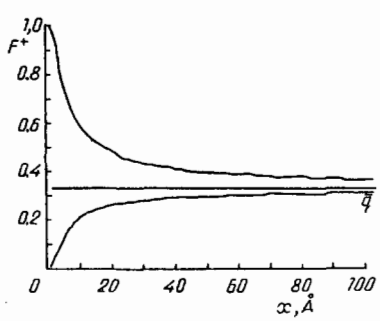

FIG. 2. Variation of charge state (F^+ is fraction of ions in beams, $\bar{q}$ is the equilibrium value) of beams of H (upper curve) and H^+ (lower) ($E = 6$ keV), passing through gold target.[7]

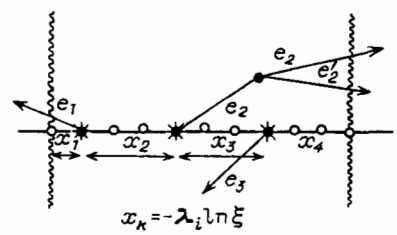

FIG. 3. Qualitative picture of the passage of a high-energy particle through target material. x_k is the path traversed by particle between successive ionization events—production of electrons e_k; e_k'—cascade electron.

to an escape asymmetry in the laboratory system, the degree of which is determined by the ratio of the velocities (or energies) of the electron and heavy particle. Let us point out that this kinematic model may be untenable for electrons with energies $E_e > 100$ eV. (Measurements of the angular distributions of electrons ejected in collisions of protons in gaseous targets[8] also indicate this.)

The migration of the internal secondary electrons in the target material will be accompanied by individual and collective interaction processes. Individual collisions lead to elastic scattering—a change in trajectory- (with a cross section of Q_{el}), inelastic collisions—a slowing of the electrons (cross section Q_{in}), and to direct ionization—a cascaded multiplication of electrons (cross section Q_{ie}). The slowing of the internal secondary electrons in the case of collective interactions is attributable to electron–phonon scattering and the production of plasmons. As follows from Fig. 4, an electron arriving at the target-vacuum interface has the possibility of escaping by surmounting the surface potential barrier. For the simple model of a plane surface barrier the escape conditions are shown in Fig. 4, and one can see from them that passage through the barrier modifies the angular and energy distributions of the emitted secondary electrons from that of the low-energy population of internal secondary electrons. Within the framework of the picture of the secondary emission process being considered it must be expected that the electron emission statistics will be determined by a superposition of a Poisson distribution of true secondary electrons produced by ionization and the distribution of the electrons produced by cascade. It is also clear that a correlation of the forward/backward yields can be interpreted as indicating multielectron ionization of the atoms of the target material.

2. METHODOLOGICAL ASPECTS

One of the fundamental methodological achievements of recent investigations is the widespread use of thin targets—foils, which provide the following advantages:

1. The losses of particles passing through the target are reduced to a negligible level—the collisions are monoenergetic.

2. By varying the target thickness one can obtain conditions for which the characteristic ranges for different collisional processes (ionization by recoil atoms, multiple ionization) occur at larger thicknesses, and in this way their contribution to the secondary emission flux will be suppressed.

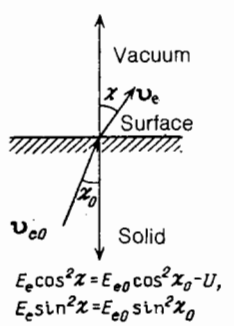

FIG. 4. Diagram of plane surface of potential barrier of height U.

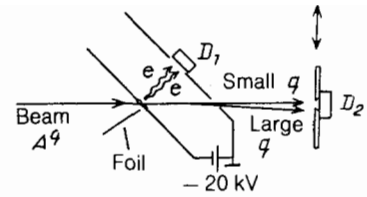

FIG. 5. Apparatus for studying statistics of one-sided (transmission) emission from a carbon foil.[9] D_1, D_2 are semiconductor detectors of the secondaries Se and of the primary beam, respectively. The foil is inclined at 45° to the beam.

3. The yield asymmetry and the effects of the charge state of the particle passing through the target can be investigated.

4. An important advantage is associated with the possibility of an independent measurement of the absolute intensity of the beam passing through the target, which usually involves difficulties, especially in the case of neutral atoms.

A complicating factor in measurements on thin targets is the dependence of the measured effect (for example, the average yield) on the thickness d, making it a difficult problem to compare measurements made in different laboratories. A simple scaling of the measurement results to the foil thickness will not be justified in all cases (especially for $d \sim \lambda_e$).

Figure 5 shows a diagram of an apparatus for investigating the statistics of multielectron secondary emission by a carbon foil, bombarded by H^+, He^+, H_2^+ ions in the 0.4–2.8 MeV energy range. The foil being investigated (650 Å thick) is mounted at a 45° angle to the beam axis, and the secondary electrons (preaccelerated to an energy of 20 keV) are detected by the semiconductor detector D_1. The configuration of the apparatus makes it possible to investigate only the yield in transmission. Let us point out that a similar configuration was used in Ref. 10, but the foil was mounted normally to the beam, and two symmetrically arranged detector units provided for an extraction at a 45° angle and collection of both transmitted and reflected electrons. As follows from Fig. 5, the particles of the primary beam are detected by the movable semiconductor detector D_2, while a special deflection system is used in this detection channel in

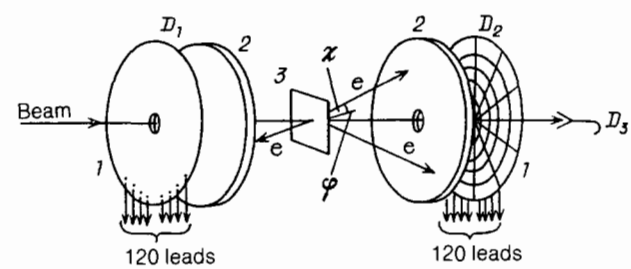

FIG. 6. Apparatus for studying statistics of two-sided emission from carbon foil—measurements of triple differential cross sections (with respect to number, energy and angle of the emitted electrons) $d^3\gamma/dk\,dE_e d\Omega_e$.[11] D_1 and D_2 are electron detectors employing microchannel plates, D_3 is the detector for the primary beam. *1*–assembly of two microchannel plates (75 mm diameter), *2*–sectored (120 elements) collector, *3*–foil perpendicular to primary beam. Diameter of holes in D_1 and D_2 is 6 mm.

order to separate according to charge state the ions leaving the foil.

The design of a fundamentally new[11] apparatus developed by these authors is shown in Fig. 6. The modification had the purpose of making it possible to analyze simultaneously the reflected and transmitted secondary electrons according to number, energy and escape angle, i.e., this modification made it possible to measure the triple differential cross section.

The foil (of various thicknesses, 140, 500, and 1000 Å) is mounted perpendicularly to the beam, and special detectors, having both time and spatial resolution, are used for simultaneous measurements of the angles and velocities of the emitted electrons. The detectors are based on an assembly of two microchannel plates with a sectored anode.

Holes (6 mm in diameter) are made in the channel plates and collector for the passage of the primary beam, and the latter is received by the special detector D_3 employing a channel electron multiplier. The spatial resolution of the detectors D_1 and D_2 is provided by the multielement structure of the collector (120 independent elements, formed from 10 concentric annular strips, each of which is cut into 12 sectors). The energy analysis of slow secondary electrons is accomplished by measuring the transit time from the foil to the detectors (D_1, D_2). The signal of an electron arrival is used as the start signal and the delayed signal from D_3 is the stop. Depending on the point of electron impact on the surface of the MCP (75 mm diameter) a signal appears at one of the 120 collector elements, the address of which encodes the escape angles (χ, φ) of the electron. For multielectron events the transverse components of the electron velocities provide for such a spread of electrons that a number of collector elements are activated. The automated measurement system provides for the simultaneous interrogation of all elements, so that there are essentially no constraints on the number of electrons that can be recorded in a MUSE event. The energy range of the secondary emission measurements is restricted by the obvious condition $v_t \gg v_e$ (t is the heavy primary particle and e is the electron); there are no such constraints on the angular measurements.

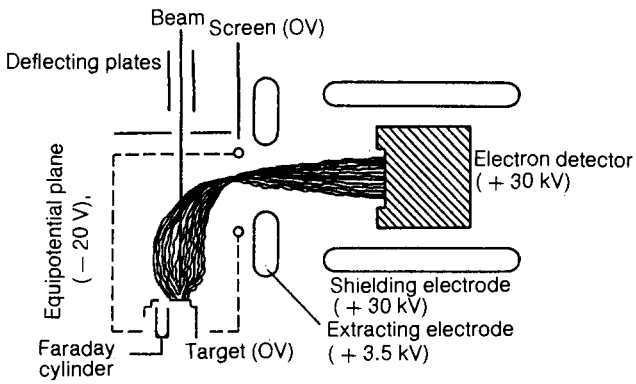

FIG. 7. Apparatus for studying secondary emission statistics of a massive gold target.[12] Electrons, extracted to detector (the beam of calculated trajectories with $E_e = 20$ eV is shown) are accelerated to an energy of 30 keV. Deflection plates are used to draw the primary beam into the Faraday cylinder and to deflect the ions for bombardment of the target with atom beams. Target is connected in a circuit for measuring a current containing ion and electron components.

The diagram of an apparatus[12] for investigating emission statistics from a massive target bombarded by various beams with energies in the 1–16 keV interval is shown in Fig. 7. A semiconductor (silicon) detector is used to detect the secondary electrons, which are accelerated to an energy of 30 keV. A typical amplitude spectrum is shown in Fig. 8, and the successive peaks correspond to energy dissipated in the simultaneous arrival at the detector of k electrons, each delivering an energy of 30 keV to the SCD.

As is seen, the peaks are well separated ($\Delta E_{1/2} = 6$ keV), and the only problem in interpreting the experimental spectra is that of eliminating the overlapping near the bases of the peaks. These overlap areas are caused by energy losses in the reflection of some of the detected electrons from the silicon surface and the protective Al layer of the silicon detector. As a result of the reflections, the energy of this portion of the detected electrons in each peak is reduced and will be characterized by some distribution. If this effect is taken into consideration by using data on the slowing losses of electrons it is possible to separate completely the contributions of the peaks belonging to different values of k. The calculated profiles of the lines corresponding to $k = 2$, 4, and 6 are shown shaded in Fig. 8, and on the basis of such a processing of the raw spectra one can find the true number of events in which a given number k of electrons are emitted.

Measurements were made under ultrahigh vacuum conditions ($p \leqslant 2 \times 10^{-10}$ mb), and the polycrystalline gold target was subjected to ion etching in order to obtain an atomically clean surface. Beams of H, H_2, H_3 and ions of noble gases in various charge states ($q = 0, \pm 1, +n$) were used for the bombardment in the measurements.

Figure 9 shows the diagram of an apparatus for investigating the secondary emission statistics of a thin foil,[13] making it possible to record the secondary electrons independently and for the case of coinciding outputs from both sides.

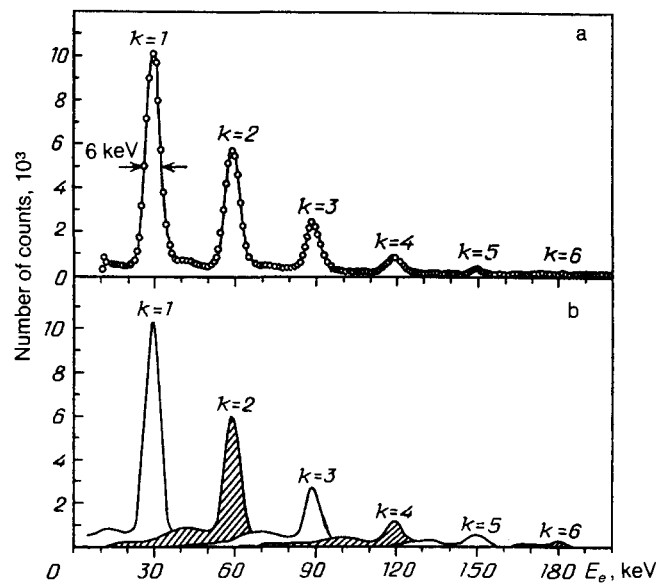

FIG. 8. Typical amplitude spectra of signals of the semiconductor detector for the apparatus shown in Fig. 7. a–Measured spectrum.[12] b–Result of decomposing the measured spectrum into multiple peaks with the internal reflections of the detected electron groups in silicon detector taken into account (shaded areas indicate true shape of peak for $k = 2$, 4 and 6).

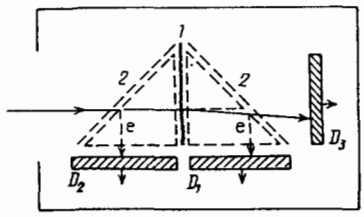

FIG. 9. Apparatus for studying the statistics of the two-sided emission from a thin target.[13] *1*–foil, *2*–electrostatic mirror for the acceleration and extraction of the electrons from the trajectory of the primary beam. D_1, D_2 are detectors (employing microchannel plates) of the electrons leaving by transmission and by reflection. D_3 is the detector of the primary beam using a VÉU-7 electron multiplier. $D_1 - D_3$ can operate independently and in coincidence. The trajectory of a secondary electron is shown by the dashed line.

The principal elements of the instrument are two identical electrostatic mirrors 2, which accelerate and transport isochronously to the detectors D_1 and D_2 the electrons leaving from an arbitrary point of the foil. The mirrors, fabricated from high-transmission ($\gtrsim 95\%$) grids, in addition to extracting the electrons from the axis of the primary beam (the trajectories of the accelerated electrons are turned by 90°), image the emission plane (foil) onto the entry plane of the detectors D_1 and D_2. The acceleration of the electrons (to an energy of ~ 1 keV) suppresses the transverse velocity components, and produces a transverse deflection of the impact point of an electron arriving at the detector relative to the exit point in the emission plane. This imaging property of the detection system in combination with the use of position-sensitive detectors can be extremely useful for working with wide-aperture beams, characteristic of a number of diagnostic problems involving hot plasmas in a laboratory or space[14] environment. An ultrathin (~ 50 Å) carbon foil was used in the instrument being discussed. The uniformity of the foil composition and thickness were investigated on other samples (fabricated using the same technology) by Rutherford backscattering and by other methods.[15] The specially constructed[16] detectors D_1 and D_2 employing microchannel plates have narrow single-electron amplitude distributions (a resolution of $R_A = 30$–40%, where $R_A = \Delta A / A_{max}$ A_{max} is the most probable signal amplitude, and ΔA is the full width of the signal amplitude distribution at the half-height. The detectors, operating in the counting mode (the intensity of the primary beam was $I_0 \sim 10^3$ sec^{-1}), make it possible to determine reliably for each emission event the number of electrons arriving at the detectors—the amplitudes A_1, A_2 of the signals of D_1, D_2 are proportional to the number of arriving electrons. The third detector D_3 (VÉU-7 type) serves to detect particles of the primary beam passing through the foil.

The three detectors D_1, D_2, D_3 can operate independently and in coincidence (pairs, triples). Recording of the coincidences D_1-D_2 makes it possible to investigate directly the correlation of the events.

The simple ratio[17] $I_0 = I_{1,2} I_3 / I_{1,2-3}$ (here I_1, I_2, I_3 are the counting rates of the detectors D_1, D_2, D_3 and $I_{1,2-3}$ are the counting rates of the corresponding coincidences) was used to determine the absolute intensity I_0 of the primary beam. The automated recording system was constructed out of CAMAC modules, operating under the control of a microcomputer. Pulse-height analyzers were also used. The neutral component of the ion beam from a linear accelerator (charge transfer to residual gas with deflection of the non-neutralized ions) was used to obtain beams of high-energy atoms.

Figure 10 shows typical multielectron secondary emission yield spectra (in reflection) when the foil is bombarded by beams of sulfur atoms of various energies. The true distributions N_k of the number of electrons leaving the foil can be extracted from measured spectra of the type shown in Fig. 10a after a numerical deconvolution. Deconvolution of the experimental spectra makes it possible to resolve the overlapping peaks (see Fig. 10a) corresponding to emission events of different multipliciplicity and to take account of the losses of electrons being transported to the detectors due

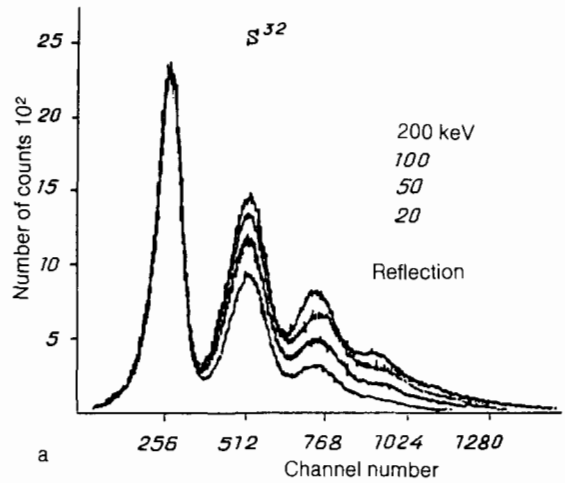

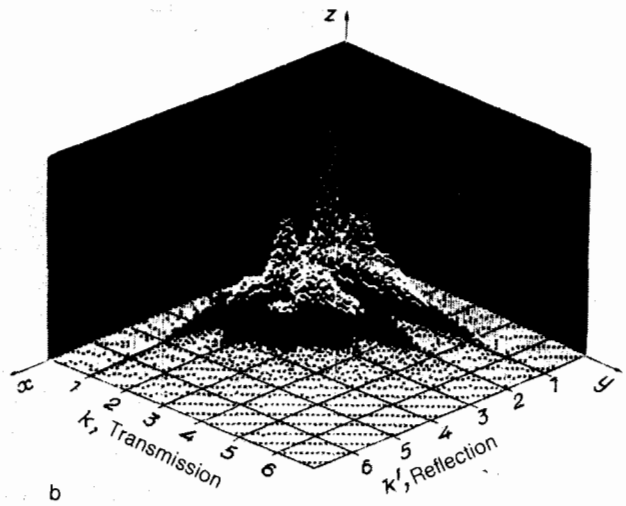

FIG. 10. Amplitude spectra typical of the apparatus in Fig. 9. a–Amplitude spectrum of secondary electron detector (beam of S, $E = 30$, 50, 100, 200 keV, reflected emission). Peaks correspond to arrival of 1, 2, 3, etc. electrons simultaneously at detector. The width of the single-electron (and other) peaks is determined by the multiplication statistics of the channel plate assembly. A numerical deconvolution of the spectrum is carried out in order to separate the peaks. b–Typical form of amplitude spectrum when recording coincidences of transmission and reflection emission events.

to the less-than-100% transmission of the grids and the deviations of the recording efficiencies of the detectors D_1 and D_2 from unity. For a known primary beam intensity I_0, one can find the absolute yields from the distributions N_k accumulated during a time τ, i.e., one can determine the values of the absolute probabilities for the emission of k electrons P_k ($= N_k/M$; $k = 1,2,3$, $M = I_0\tau$).

The probability P_0 can be found both from N_0 ($= M - \Sigma_{k=1}^{\infty} N_k$), and from the relation

$$P_0 = 1 - \sum_{k=1}^{\infty} P_k.$$

The simultaneous electron yields in transmission (k) and in reflection (k') were recorded in the measurements made in the coincidence mode. A typical spectrum of such simultaneous yields is shown in Fig. 10b. These experimental spectra must also be deconvoluted to extract the true distributions $N_{kk'}$.

The measured secondary emission yields for the two sides of the foil are not identical. A qualitative asymmetry of the secondary emission was found both in the difference of the counting rates ($I_1/I_2 > I_1$) and also in a difference in the coincidence rates for the two sides ($I_{1-3}/I_{2-3} > 1$) in all measurements. The probabilities P_k ($P_{k'}$) and $P_{kk'}$ are interrelated by an expression of the form $P_k(E) = \Sigma_{k'=0}^{\infty} P_{kk'}(E)$.

Thus the secondary emission statistics of a thin target can be investigated by measuring only $P_{kk'}(E)$. However, it is convenient to measure all three probabilities. This makes it possible to carry out a cross check of the measurements and increase the accuracy.

3. NEW RESULTS OF SECONDARY ELECTRON EMISSION INVESTIGATIONS

Here we will consider recent results that are very interesting in connection with the development of a quantitative model of the effect. This concerns measurements of the energy and angular spectra of emission electrons for different target materials and of studies of the multielectron emission statistics for carbon and gold.

3.1. Energy spectra of secondary electrons

A simple retarding-field spherical analyzer, the center of which coincides with the incidence point of the beam, normal to the plane of the target, was used in Ref. 18 to determine the energy spectra of secondary electrons, emitted during the bombardment of massive targets. The measured spectra are angle-integrated. The measurements were made under ultrahigh vacuum conditions at a pressure of $\sim 5\times 10^{-9}$ mb, and the targets were cleaned beforehand by etching with an ion beam (Ar^+).

Figure 11 shows a summary picture of the measured spectra for a set of different targets bombarded by a proton beam with $E = 500$ keV. The qualitative similarity of the spectra in Fig. 11 is also borne out by the data in Table I. An interesting feature of the spectra is the essentially constant location of the maximum for a wide interval of beam energies (50–900 keV). The half-width of the spectra also turns out to be independent of energy. This puzzling invariance of the spectra is undoubtedly a reflection of the fact that the energy spectrum of the outgoing secondary electrons is determined by the height U of the surface potential barrier and by the

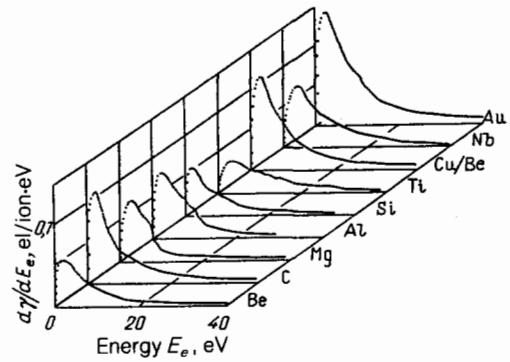

FIG. 11. Panorama of energy spectra obtained in Ref. 23 for bombardment of different targets by a proton beam ($E = 500$ keV). Note the qualitative (and quantitative: see Table I) similarity of the spectra.

energy distribution of the internal secondary electrons in the region $E_e > U$. In the absence of a nonempirical theory, a hint at the nature of this similarity of the spectra can be seen in the results of measurements of the angular and energy spectra of electrons resulting from the collisions of high-energy protons in gas targets.[8,19] At energies E_e extending to $E_e = m_e v_T^2$ it follows from these measurements that in a first approximation the spectrum can be approximated by a universal curve of the form $d\gamma/dE_e = \text{const}\cdot(E_e + I)^{-2}$ ($d\gamma/dE_e$ is the differential cross section of the formation of an electron with energy E_e and I is the binding energy of the freed electron). Thus one can expect that for a collisional generation mechanism the "genetic attributes" of the secondary electrons should be suppressed both by the presence of the potential barrier and also by the weak effect of I on the spectrum in the factor of the form $(E_e + I)^{-a}$ in the $E_e > I$ region ($a = 2$ for protons).

Figure 12 shows the energy spectra of electrons for different emission angles in the front hemisphere. Measurements have been made[20] with a proton beam ($E = 170$ keV) bombarding a thin (100 Å) carbon foil. Let us point out two features of the spectra shown. These are an output of convoy electrons (the narrow peak at $v_e \approx v_t$) for angles close to $\chi = 0°$, and the kinematic cutting-off of the spectrum (for $E_e > 400$ eV). The energy spectra of electrons emerging at an angle of $\chi = 180°$ (reflected) for H^+ and H beams with an energy of 100 keV are shown in Fig. 13. In the overall similarity of the spectrum, the reader should note the difference in the vicinity of the convoy peak for $v_e \approx v_t$: for the beam of

TABLE I. Energy E_{max} at maximum and half-width of energy spectrum for targets bombarded by protons with $E = 500$ keV.[18]

Target	E_{max} (± 0,2), eV	$\Delta E_{1/2}$ (± 0,4), eV
Be	2,0	6,8
C	2,0	5,4
Mg	3,0	6,0
Al	2,0	8,2
Si	1,8	6,2
Ti	3,4	11,8
Cu/Be	2,4	6,8
Nb	3,6	9
Au	2,2	8,4

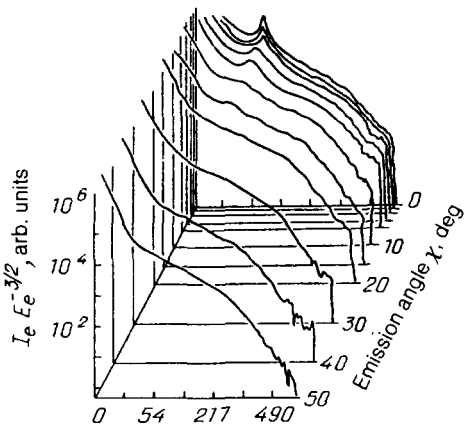

FIG. 12. Double differential cross section $d^2\gamma/dE_e d\Omega_e$ of transmission electron emission for bombardment of carbon foil (100 Å) by beam of protons with energy of $E = 170$ keV.[20] The peak on the distributions in a narrow cone near $\chi = 0$ corresponds to the contribution of convoy electrons with $v_e = v_t$. The product of the electron counting rate I_e times $E_e^{-3/2}$ is plotted along the vertical axis; this makes it possible to compensate for the rapid change in the instrument function of spectrometer with an increase in E_e. The horizontal axis is linear in the velocity v_e, but the energies E_e in eV are indicated along it.

H atoms the yield fraction within the limits of the convoy peak is considerably greater than for the H^+ peak. This difference is unambiguously due to ionization of the H atoms within the target. A direct confirmation of this is found in measurements of the probabilities $P_{k'}$ of reflected emission.[22] When a carbon foil is bombarded by beams of H atoms or protons with energies of 20–200 keV, the $P_{k'}$ values (for $k' \geqslant 1$) are found to be 10–15% higher for H than for H^+.

3.2. Average secondary electron yield

Measurements of the total yield of electrons (per ion) have been and are still the most popular among secondary emission investigations. Here, in addition to the traditional current measurements (the ion currents J_i and the secondary electron currents J_e) giving the quantity $\gamma = J_e/J_i$, the total yield can be determined from measurements of the probabilities P_k. In this case we will denote the yield by $\bar{k} = \sum_{k=1}^{\infty} kP_k$.

Figure 14 shows the energy dependences of the total yields ($\bar{k}'$ for reflection and $\bar{k}$ for transmission) of electrons for bombardment of a carbon foil by beams of hydrogen (H), helium (He), oxygen (O), and sulfur (S) atoms.[21,22] Note that the $\bar{k}(E)$ relationship passes through a maximum for H; for the other peaks the position of the maximum should be shifted to energy values that are a factor of m_A/m_H higher than for the E_{max} value for H atoms. The $\bar{k}(E)$ behavior reproduces qualitatively the behavior of the stopping power $(dE/dx)_e$. The similarity, however, is misleading. Actually, in the case of the H beam the values of $(dE/dx)_e$ will be identical for $E = 20$ keV and $E = 200$ keV, but neither $\bar{k}$, $\bar{k}'$ nor the partial yields P_k, $P_{k'}$ turn out to be identical there.

The absolute values of $\gamma(E)$ and $\bar{k}(E)$ depend on the thickness of the foil being used, and in the absence of any reliable data on λ_e—the escape depth of the secondary electrons—scaling of the measurements is extremely difficult; a simple normalization at the overlapping values of the beam energy will be the best approach in this case.

The primary objective of wide-band measurements of $\gamma(E)$ is related to attempts to find a universal relationship that could serve as a basis for the theoretical concepts that are developed and as a quantitative prediction of γ for uninvestigated systems. The most comprehensive systematization of measurements for a carbon target has been made in Ref. 24 and its results are shown in Fig. 15. The measurements encompass the $15–16 \times 10^3$ keV/amu energy range and the $1 \leqslant Z_A \leqslant 92$ range of atomic numbers of the bombarding ions. The set of measurements plotted as γ vs $(dE/dx)_e$ can actually be approximated by a straight line. Here the average value $\gamma/(dE/dx)_e = \Lambda^* = 0.31$ Å/eV is found. The quantity Λ^* is usually called a parameter of the material (carbon in this case), and the single value $(\Lambda^*)^{-1} = 3.2$ eV/Å characterizes the ionization losses along a 1-Å path

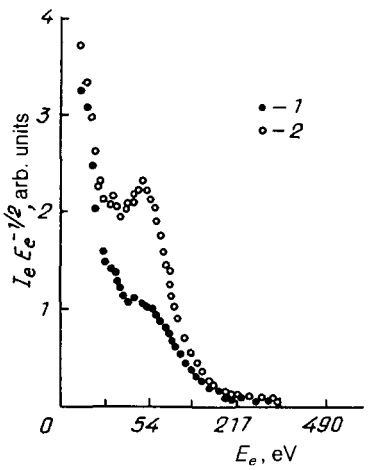

FIG. 13. Energy spectrum of electrons leaving a carbon foil (100 Å) at an angle $\chi = 180°$ for bombardment by beams of protons (*1*) and hydrogen atoms (*2*) with an energy of 100 keV.[20] In the case of the atom beam the quasiconvoy component ($v_e \approx v_t$), caused by ionization of H atoms in the target, has been separated out. A value proportional to $(d\gamma/dE_e)E_e^{1/2}$ is plotted along the vertical axis, and the horizontal axis is linear in the velocity v_e.

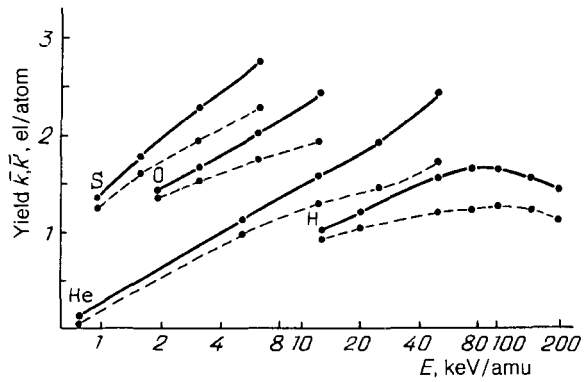

FIG. 14. Dependence of the total forward $\bar{k}$ yields (solid lines) and backward $\bar{k}'$ yields (dashed lines) on energy for H, He, O, S beams, bombarding a thin (~50 Å) carbon foil. A maximum is clearly detected in the case of the H atoms, correlating with the location of the maximum in stopping power. Lines joining the experimental values are drawn for convenience.

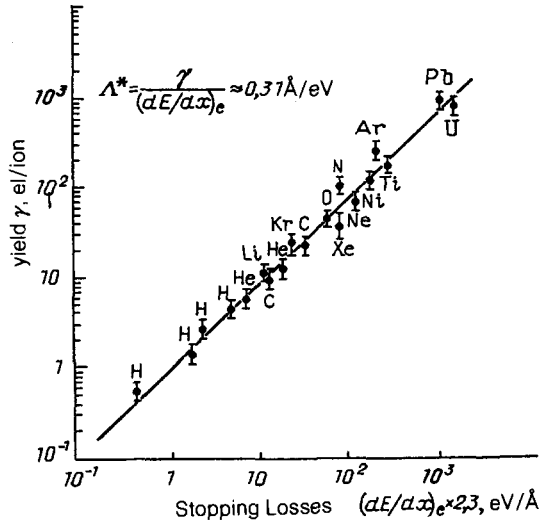

FIG. 15. Correlation of measurements of the total secondary electron yield γ for bombardment by various beams of ions with the value of the stopping power $(dE/dx)_e$, calculated for the beam energy used in the measurements of Ref. 22.

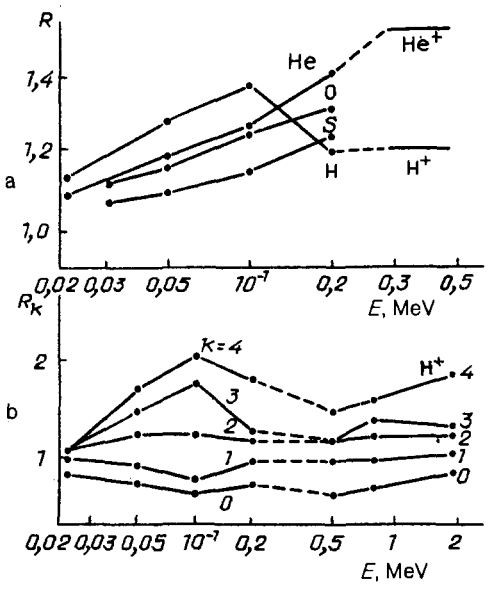

FIG. 16. Asymmetry of secondary yield for a carbon foil bombarded by atom beams of different energy. a–Asymmetry of total yields, $R = \bar{k}/\bar{k}'$; data are for H^+ and He^+ for $E > 0.3$ MeV from Ref. 24; dashed lines represent interpolation. b–Asymmetry of partial yields, $R_k = P_k/P_{k'}$, for H and H^+; data for protons from Ref. 11; dashed lines represent interpolation.

for one emitted electron.

However, plotting the data on a log–log scale in Fig. 15 conceals deviations of the measurements from the approximating straight line (the errors of the γ measurements can be indicated while the errors in the calculated values of the stopping power are indeterminate), and predictions of the expected yields for other systems may be accompanied by errors. In investigations with other targets[25] of Au, Ag, Cu, Al, large systematic deviations from a constant value of $\gamma/(dE/dx)_e$ are observed with a change in the energy of the H^+ and Ar^+ beams.

Thus it appears that scaling of the integrated secondary electron emission characteristic γ by means of the stopping power $(dE/dx)_e$, although convenient, will scarcely permit progress towards a quantitative theory because of possible changes in the internal electron generation mechanisms themselves. A comparison of the value of the parameter Λ, obtained for protons in measurements[26] with carbon ($\Lambda = 0.53$ Å/eV), with the average value of $\Lambda^* = 0.31$ Å/eV (see Fig. 15) is indicative of this difficulty.

In investigations with thin targets, one of the results of measuring the total yield is a determination of the yield asymmetry $R(E)$, i.e., the ratio of the transmission yield to the reflection yields $R(E) = \gamma(E)/\gamma'(E) = \bar{k}(E)/\bar{k}'(E)$. For the quantity $R(E)$ one can expect a much lower sensitivity to thickness and, thus, independent results of different authors can be compared. Figure 16a shows curves of $R(E) = \bar{k}(E)/\bar{k}'(E)$ from the data of investigations[21] with H, He, O, S atoms. Values for H^+ and He^+ for current measurements $R = \gamma/\gamma'$ at higher energies ($E \geqslant 300$ keV) and a foil thickness of 10^3 Å from Ref. 24 are also shown there. As seen from the shape of the dashed interpolating lines in Fig. 16, the agreement is completely satisfactory. It is perfectly natural that the asymmetry of the total yield is comprised of the partial asymmetries R_k, and experimentally determined $R_k = P_k/P_{k'}$ dependences[11,21] are shown in Fig. 16b. In this case data for different foil thicknesses also turn out to agree well and they provide a basis for conclusions about the features of collision processes of generation and transport of internal electrons.

3.3. Multi-electron secondary emission statistics

Recently performed measurements of the distributions of the absolute yield probabilities $P_k(E)$—multi-electron secondary emission statistics for C and Au targets—make it possible to draw quite definite conclusions about the mechanisms responsible for the formation of the secondary electrons. Typical histograms of probability distributions $P_k(E)$, $P_{k'}(E)$, $P_{kk'}(E)$ are shown in Figs. 17–19. The existence of data on the probabilities P_k makes it possible to analyze the type of multi-electron secondary emission statistics. The generalized outcome of such an analysis, illustrated in Figs. 18 and 19, reduces to the fact that the experimentally determined distributions of P_k and $P_{k'}$ are not described by a Poisson distribution. A comparison with the Poisson distribution, calculated from the value of $\bar{k}$, is shown in Fig. 18 for the case of a beam of S atoms, while the dependences of γ on the ratio P_k/P_{k-1}, obtained in measurements with beams of H^+, He^+, Ne^+, Ar^+ ions bombarding a gold target,[27] are shown in Fig. 19. Let us recall that for a Poisson distribution $P_k/P_{k-1} = \gamma/k$ and, consequently, the $\gamma(P_k/P_{k-1})$ dependence should be linear. As seen from Fig. 19, the curves approximating the measurements can in no way be identified with a linear dependence, and it is on this basis that one must conclude that it is impossible to use the Poisson law to describe the experimental data.

A search for other theoretical distributions (for example, a Pólya distribution), which could formally describe observations, does not appear to be very promising. It would be more fruitful to look for the physical reasons for "deformation" of the experimental distributions from a Poisson

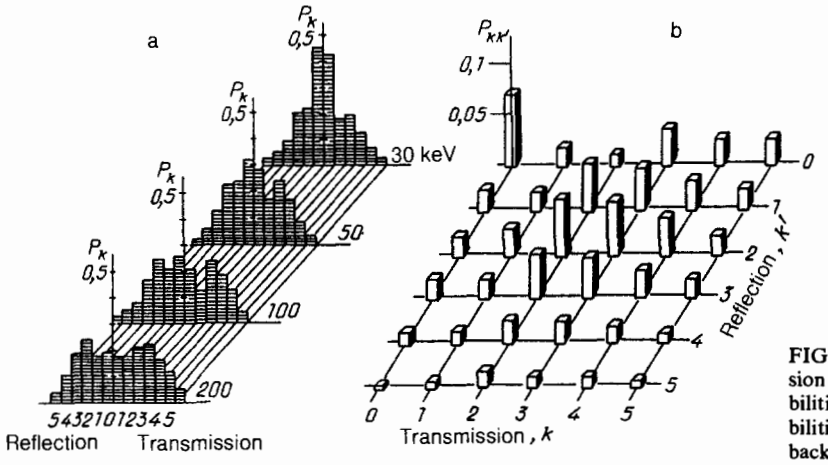

FIG. 17. Probability distributions of one- and two-sided emission of a thin carbon foil bombarded by sulfur atoms. a–Probabilities $P_{k'}$ and P_k of reflection and transmission yield. b–Probabilities $P_{kk'}$ of simultaneous yield k, k' of electrons forward and backward.

distribution, dictated by the obvious statistical nature of the generation of internal secondary electrons by a fast particle passing through a material. As is known,[28] a random filtering of a Poisson flux (for example, by a transport process) preserves the original distribution type, and the deviations found in experiments must be naturally related to the operation of additional mechanisms for the formation of internal secondary electrons. Possible candidates for the role of such processes are cascade multiplication in electron–atom collisions in the material and ionization by recoil atoms.

The probabilities of the two-sided yields $P_{kk'}$ also reveal a specific asymmetry. Thus for nonidentical values $k \neq k'$ giving the same total charge $q = k + k'$, the probability $P_{kk'}$ with $k > k'$ exceeds that with $k < k'$. In the case of a thin target the probability P_{00} is the result of two contributions—from passage through the target without the generation of secondary electrons and from passage through the target with the production and loss of electrons. The probability of realizing the first case is given by $\exp(-d/\lambda_i)$, and in a rough approximation, ignoring the second contribution, one can estimate the upper limit of λ_i from the measured P_{00}. More precise results can be obtained in a numerical modeling of the statistics by the Monte Carlo method.

Using $P_{kk'}$ values found from measurements, one can find the correlation coefficients $\rho_{kk'}$ of the probabilities P_k and $P_{k'}$:

$$\rho_{kk'} = (P_{kk'} - P_k P_{k'})[P_k(1 - P_k)P_{k'}(1 - P_{k'})]^{-1/2}$$

and the so-called sampling correlation coefficient $\hat{\rho}$ of the emitted charges:

$$\hat{\rho} = \frac{\sum_{k,k'} P_{kk'}(k - \bar{k})(k' - \bar{k}')}{[\sum_k P_k(k - \bar{k})^2]^{1/2}[\sum_{k'} P_{k'}(k' - \bar{k}')^2]^{1/2}}.$$

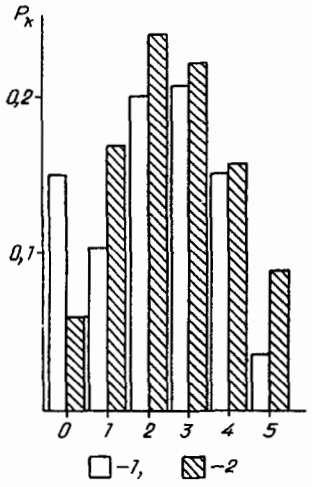

FIG. 18. Comparison of probability distributions, measured and calculated from the Poisson formula (for $\bar{k} = \Sigma_{k=1}^{\infty} kP_k$), of transmission emission for a carbon foil bombarded by beam of S atoms with energy $E = 200$ keV. *1*–experiment, *2*–calculation.

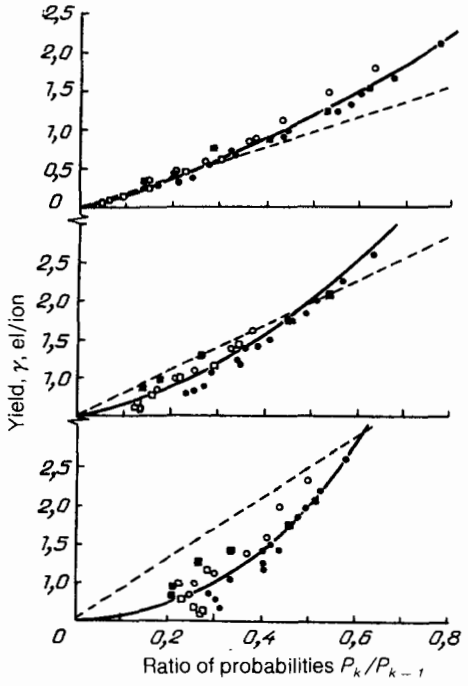

FIG. 19. Comparison of dependence of experimental[27] values of P_k/P_{k-1} on the measured value of the yield γ. From top to bottom: P_2/P_1, P_3/P_2, P_4/P_3. The curved line is polynomial approximation of experimental values; dashed lines are linear dependences corresponding to the Poisson law.

It turns out that $\hat{\rho} \lesssim 0.2$ for all systems investigated in Ref. 21. Since the primary contribution to $\hat{\rho}$ is due to the probability P_{00}, one can conclude that no appreciable correlation of the charges leaving on opposite sides exists. The probability correlations $\rho_{kk'}$ have significant values ($\lesssim 0.4$) (Fig. 20) only for $k = k' = 0$, i.e., for "nonproductive" transmissions of the foil. From the established fact that there is no correlation of the yields it must be concluded that the production events of individual internal secondary electrons are independent, i.e., multiple ionization processes of the atoms of a thin target, used in Ref. 21, make no contributions.

3.4. Molecular and charge effects in secondary electron emission

The possibilities of investigating statistics of secondary emission in the bombardment with atomic particles in different charge states (for example, H, H^-, H^+) and by homonuclear molecular ions (for example, He_2^+, H_3^+) make it possible to establish a number of fine details of the collision processes responsible for the secondary electron yield.

A study of molecular effects manifested in the additivity of the contributions of atomic particles forming the molecular ion was conducted on the basis of measurements of the total yields γ.[29] However, the additivity found earlier can be examined in greater detail by using data on emission statistics for molecular ions and corresponding fragments of the same velocity. The additivity effect, in essence, is one manifestation of the "Coulomb explosion" effect, which is well-known and is finding interesting application (see citations in Ref. 30). The term "Coulomb explosion" describes the process of removal of the outer electrons of atoms comprising a polyatomic molecule, as a result of which the interaction of fragments becomes a Coulomb repulsion. Coulomb repulsion determines the transverse scattering velocities of fragments moving in a substance at longitudinal velocities equal to the velocity of the original molecule. As a result of this scattering a unique "shower" of independently moving fragments is formed.

The idea of the independence of the generation processes of internal electrons by fragments underlies the notion of additivity. In the special case of the molecule A-B decaying into the fragments A and B upon entering a material one can write

$$P_k(\mathrm{A}-\mathrm{B}) = \sum_{i=0}^{k} P_i(\mathrm{A}) \cdot P_{k-i}(\mathrm{B}).$$

It is this relation that makes it possible to synthesize the model distribution P_k (A-B), which can be compared with the measured distribution; in the comparison the charges of the fragments A, B can be varied. Figure 21 shows the results of such a comparison for the case of the H_3^+ ion. As is seen, the model distribution is indeed sensitive to the charge state of the fragments, and a combination can be chosen that reproduces very well the direct measurements. These comparisons once again emphasize the adequacy of the collision mechanism for the generation of internal secondary electrons, and the possibility of better agreement for the H-H-H^+ combination than with H^+-H^+-H^+ is completely consistent with the expectation that the cross section of the collisional dissociation of H_3^+ exceeds the cross section of dissociative ionization. Investigations of this type can be expanded through the use of clusters (for example, atoms of noble gases), for which the large initial interatomic distances ensure the independence of the ionizing action of the fragments.

Let us point out that studies of the yields of secondary electron emission caused by bombardment with clusters, have been carried out.[31] They have found a somewhat unexpected diagnostic application in the study of the D–D fusion, induced by the bombardment of deuterated targets by accelerated clusters of heavy water $(D_2O)_n$.[32]

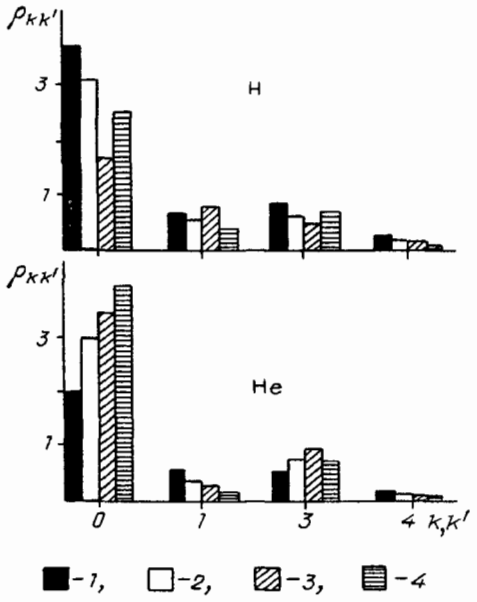

FIG. 20. Histograms of correlation coefficients $\rho_{kk'}$ of the probabilities P_k and $P_{k'}$ for H and He, bombarding a thin ($\sim$50 Å) carbon foil. The beam energies are denoted in the following manner: 1–20, 2–50, 3–100, 4–200 keV (scale along vertical axis is 10 times smaller than indicated).

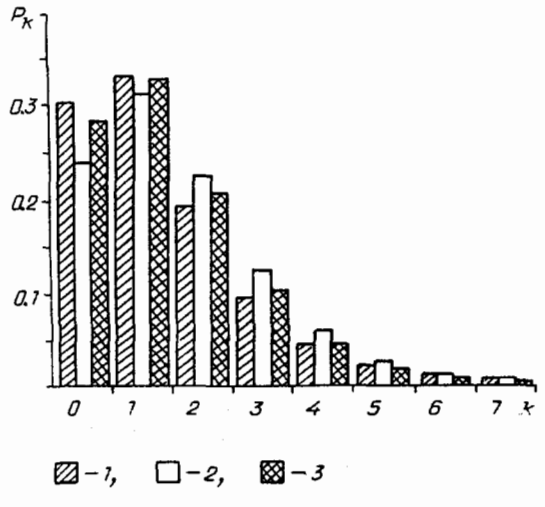

FIG. 21. Molecular effect in secondary electron emission—comparison of emission probability distributions P_k for gold, bombarded by a beam of H_3^+ ions, calculated in the additive approximation. *1*–experiment. *2*–calculation for H^+-H^+-H^+. *3*–calculation for H-H-H^+.[33]

Electron effects in secondary emission, i.e., the effect of the charge state on the total and partial yields, is clearly illustrated[33] in Fig. 22. A comparison of the probabilities for the three charge states reveals an extremely interesting feature—an appreciable relative decrease of P_0 for H^- as one goes from an energy $E = 4$ keV to $E = 16$ keV. The fairly obvious physical reason for this result is the fact that the energy of the excess electron $E_e = m_e E/m_H$ in the first case lies below and in the second case lies above the threshold of electron electron emission. The breakup of H^-—the detachment of the electron near the target surface and, correspondingly, the turn-on of this channel—also leads to the suppression of the quantity P_0 for negative ions.

Studies of the statistics of secondary emission caused by bombardment with multiply charged ions, open up interesting prospects for studying the phenomenon of potential emission. In the usual investigations with high-energy beams the measured yields (Fig. 23) are comprised of the secondary yields of two channels—potential and kinetic. The fact that the charge q of the ion is specified "at infinity," and that near the surface it can be neutralized, changing the charge, is a recognized difficulty. Thus the observed kinetic emission is caused by an ion whose charge state still must be defined more accurately. An obvious way of separating the kinetic and potential secondary yields is to reduce the energy of the bombarding particles to the level where the kinetic channel is completely shut off. Such investigations appear to be promising.

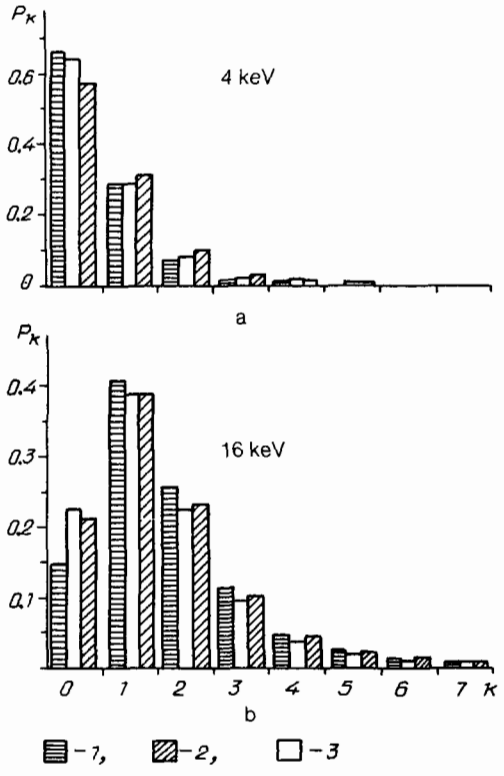

FIG. 22. Electron effect in secondary emission—effect of the charge state of particles on the emission statistics of gold, bombarded by hydrogen atoms and ions. a–Beam energy $E = 4$ keV. b–Energy $E = 16$ keV.[7] 1–H^-, 2–H^+, 3–H^0.

4. THE POSSIBILITIES OF A QUANTITATIVE DESCRIPTION OF MULTI-ELECTRON SECONDARY EMISSION EFFECTS

Because of the multistage nature of the secondary emission process one can scarcely count on developing a closed nonempirical quantitative theory. The introduction of models is unavoidable, and the adequacy of these models must be established by a comparison of their predictions with observations.

The processes caused by the passage of a high-energy particle through a substance and that terminate in the emission of secondary electrons represent a "black box" situation. Actually, we have complete (in principle) information about the initial and final state of the system, but the contributions of the processes responsible for the observed emission must be reconstructed on the basis of the model being used. It appears that the collisional model of secondary electron emission is the most obvious from a physical viewpoint. Within the framework of this model the collisional ionization of target atoms is the source of the internal secondary electrons, whose transport in the material is also governed primarily by collisions with atoms of the material (or with free electrons in the case of a metal).

Of the three stages of secondary emission discussed, the first two—the generation and transport of the internal secondary electrons—also attract the most attention in other models.[3,34] In theoretical treatments of the generation process the exaggerated evaluation of the capabilities of a quantitative description come from the use of the value of the stopping losses $(dE/dx)_e$ in the material or the value of the related inverse specific ionization loss $\Lambda = \gamma/(dE/dx)_e$. ($\Lambda$ is a parameter of the material).

The stopping loss certainly subsumes some integrated information about inelastic losses (including ionization losses) in the material, but by restricting consideration to this quantity, such key factors as the angular and energy spectra of "fresh" internal secondary electrons remain completely undetermined. If consideration is given to the fact that there exists an ever expanding reservoir of experimental and theoretical data on collisional ionization process in gases, a limitation to the stopping effect appears to be unjusti-

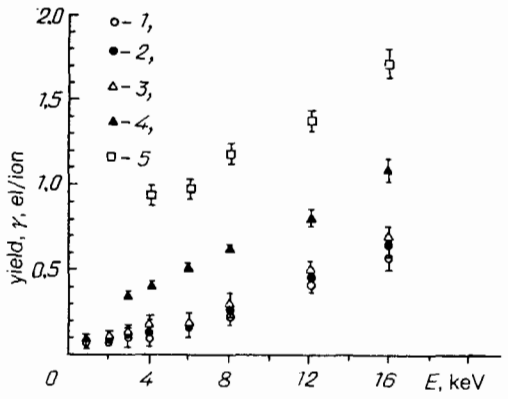

FIG. 23. Variation of $\gamma(E)$ for a gold target, bombarded by argon atoms and Ar^{q+} ions of different charge.[7] 1–Ar, 2–Ar^+, 3–Ar^{2+}, 4–Ar^{3+}, 5–Ar^{4+}.

fied. This phenomenological approach can be abandoned in favor of a collisional model of the generation of internal electrons—here a comparison of experimental data of the physics of atomic collisions with secondary emission data should lead to a realistic model of a solid as an ensemble of quasifree atoms. For such a model, providing a quantitative description of the first stage of the secondary electron emission process, the artificial isolation from the essentially boundless and still-expanding base of data of the physics of atomic (and electron) collisions will be overcome.

Problems of the second stage of the secondary electron emission process are solved most completely and coherently within the framework of the so-called Schou transport model.[34,35] A fairly detailed description and discussion of the theory have recently appeared in Ref. 3. The theory is able to predict the general form of behavior for several measured parameters (See Fig. 1), but it does not give their absolute values.[35] It allows to a certain degree a synthesis of the achievements of the kinetic description of the electron transport process and the data of the physics of atomic collisions, referring to a quantitative description of the primary characteristics of the interaction of atomic particles. This synthesis possibility appears to be the most promising one for the development of a theory. In the case of thin targets the transport theory has the following unsolved problems. First, in the treatment of the transport (and, correspondingly, the yield of electrons), only inelastic interaction processes of the internal secondary electrons are taken into account. However, it is obvious that the angular distribution of the emitted secondaries will be shaped to a considerable degree by elastic collisions of electrons in the material in different ways, depending on the thickness, washing out any possible anisotropy of the initial angular distribution of the produced electrons. Second, within the framework of the transport theory no approach has yet been developed that describes the statistics of the secondary yield. It appears that these defects of the theory are not innate, and they can be overcome as the theory evolves.

In the absence of a closed quantitative theory of multielectron secondary emission, the best possibilities are associated with a direct numerical modeling of the transport process of heavy (atoms) and light (electrons) particles in a material by the Monte Carlo method.

By introducing the effective ionization cross sections Q_i and the ionization paths λ_i, as discussed in connection with Fig. 3, the first—ionization—stage of the secondary emission process can be modeled within the approximation that the trajectories are rectilinear and with allowance for the change in the charge state of the particle (removal–recharging) as it passes through the target.

The second stage—the transport of the internal secondary electrons—can be modeled on the basis of a scheme of individual collisions.[36] In this scheme the target is assumed to consist of nuclear and electron subsystems, the latter consisting of electrons of the inner shells of the target atoms and the valence electrons, which form the electron gas of a solid. In this scheme one can take account of all elementary interactions—elastic scattering (in the field of the atomic nucleus), ionization of the inner shells, the excitation of electron-hole pairs, and the excitation of plasmons. It is able to take correct account of the cascade generation of electrons by the ionization and the excitation of electron-hole pairs and subsequent slowing of the resulting electrons within the target.

A computation subprogram using the partial wave method has been developed for calculating the elastic scattering cross sections of electrons, Q_{ei}, in the target material, following Ref. 37. The cross section for ionization by electrons Q_{ei} can be calculated within the framework of the classical mechanics approximation of pairwise collisions following Gryzinski.[38] Analogous subprograms have been written for describing other channels of inelastic interactions of the internal secondary electrons. An electron crosses the solid-vacuum interface in accordance with the conditions of Fig. 4.

Monte Carlo modeling on the basis of an appropriate package of programs makes it possible to obtain essentially all the experimentally recorded statistical, angular, and energy characteristics of multi-electron secondary emission. Thus, a matching of the calculations with measurements makes it possible to define the input parameters of the calculation more precisely. In essence, the inverse problem of determining the key characteristics of the collision processes responsible for the emission of electrons can be solved in this way. Moreover, quantities that are inaccessible to direct measurements, for example, the escape depth λ_e, the number of cascade electrons, etc., can also be obtained.

Let us point out that the Monte Carlo modeling of the collisional generation and transport of internal electrons, carried out for the measurement conditions of Ref. 21 (H beam and 50-Å thick carbon foil), has shown that the elastic scattering of electrons during their migration to the boundary completely smooths out the emission asymmetry that stems from the movement of the center-of-mass of the colliding atoms. Thus for such a model of the emission of "fresh" electrons the observed asymmetry of the transmission and reflection yields is not reproduced. The model of isotropic emission in the center-of-mass system must therefore be modified.

The direction in which to proceed to effect these modifications was indicated quite clearly by the results of investigations of the collisional ionization of gas targets by protons.[8] The data from measurements with different gases show that in the laboratory system the emission into the front hemisphere is described by a $\cos^l\chi$ ($l>1$) law, and in the rear hemisphere the emission is essentially isotropic in the laboratory system. Thus the quantity l, along with λ_i (or Q_i) becomes another parameter of the calculation. In connection with the parameter $Q_i(E)$, let us point out that its values can be obtained from the model of collisional ionization developed by Firsov.[39] The model, which has been well validated through comparisons with a large number of measurements in gases,[40] makes it possible to take account of the electron configuration of atoms of the target material, and it gives a reliable estimate of the values of $Q_i(E)$ for Monte Carlo calculations. According to this theory the ionization cross section can be described by the expression $Q_i(E) = Q_0[(E/E_0)^{1/10} - 1]^2$, where $E_0 = 2.7 \times 10^2 m_b I^2/(Z_b + Z_t)^{10/3}$ eV, and $Q_0 = 33(Z_b + Z_t)^{-2/3}$ Å^2; E is the energy of the beam atoms, Z_b and Z_t are the atomic numbers of the beam and target particles, and I is the ionization energy. This model has been extended in recent years[41] and it will certainly be useful for quantitative calculations of multielectron secondary emission (and quantitative predictions

in the future). Returning to the "hard" statement about the fruitlessness of using the stopping power $(dE/dx)_e$, let us point out that the Firsov theory makes it possible to calculate on a single basis not only Q_i but also energy losses during slowing in the target material.

A computational realization of the above-described scheme is illustrated in Fig. 24, in which the calculated and measured probabilities P_k are compared for the case of bombardment of a thin (50 Å) foil with 50-keV hydrogen atoms.

As is seen, even for the first approximation to the values of the input parameters for this calculation one can immediately obtain good agreement with measured values of P_k. The corresponding value of the ionization path length λ_i is 16.5 Å. Agreement is obtained (see Fig. 24) if one assumes identical path lengths λ_i for protons and hydrogen atoms, and uses the relationships for protons from Eqs. (8) and (19) for the energy and angular spectra of the generated electrons. These approximations allow for refinements, and the excess of the calculated value of P_0 over the measured value visible in Fig. 24 can be associated with the ignored contribution of the ionization of the H atom itself. Adequate agreement between calculation and measurements is also obtained for the values of $P_{kk'}$.

An interesting result of Monte Carlo modeling is the differences in the mean values and variances of the energy distribution of the electrons emitted in reflection and in transmission. It is seen from the results of the Monte Carlo modeling that the relative contribution of cascade electrons increases with k-multiplicity emission, reaching values of 30–40% for $k = 4$–5. "Switching-off" the cascade channel in the calculation severely worsens the agreement. The value of $\lambda_i = 16.5$ Å given above corresponds to an effective ionization cross section of $Q_i = (\lambda_i n)^{-1} = 6 \times 10^{-17}$ cm^2. This value correlates well with the theoretical value.[39] In the comparison one must consider that the $Q_i(E)$ are not the total, but rather the cutoff ionization cross sections (because of the surface barrier).

An estimate of the differences in the values of the total and cutoff ionization cross sections can be obtained by using the expression for the binary ionization cross section proposed in Ref. 8. A rigorous analytical estimate is a complex matter, however, because in reality restrictions on yield are imposed not only by the energy of the internal secondary electron but also by the angle at which it approaches the target-vacuum boundary. These constraints can be taken into account consistently in the Monte Carlo modeling. From the values found for λ_i it is easy to estimate the contribution of unproductive traversals. A comparison of it with the experimental value leads to the conclusion that the total probability of "traversals with loss" of the generated electrons exceeds the probability of unproductive traversals by a factor of two or three.

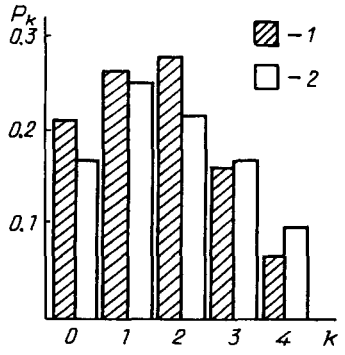

FIG. 24. Comparison of measured (*1*) distribution of partial probabilities P_k and the results of Monte Carlo calculation (*2*) for a beam of hydrogen atoms with $E = 50$ keV and an ionization path length of $\lambda_i = 16.5$ Å (foil thickness is 50 Å).

From the values found for λ_i it is easy to find the average expenditures of energy $\Delta E_i = \lambda_i (dE/dx)_e$ in the generation of one internal electron. From a comparison of ΔE_i with the energies to detach electrons, one can conclude that the average losses to ionization exceed the true ionizing losses by an appreciable amount (by a factor of four or five). These considerations indicate once more the inadequacy of describing secondary electron emission by means of the stopping losses: the principal expenditure of energy goes into electron excitation without producing electrons able to surmount the potential barrier.

By using realistic angular and energy distributions for the internal generated electrons, it is easy to obtain from Monte Carlo calculations a value of λ_e—the characteristic escape depth—that is inaccessible to reliable measurement. The quantity λ_e can be found simply from a calculation of the variations of the yield $\bar{k}$ for different depths of the hypothetical plane of electron generation within the target.

Let us also point out that a comparison of calculation and measurements imposes very severe requirements on the accuracy of the measurement of the foil thickness being used. Therefore, the 20% uncertainty in thickness existing in the present case can scarcely warrant an attempt to increase the accuracy of the calculations before removing the uncertainty in d. The fact that essentially all quantities accessible to measurement can be obtained by Monte Carlo modeling is important. Therefore, an experiment with simultaneous recording of the statistical, angular, and energy characteristics of the multi-electron secondary emission process is crucial.

It appears to be quite obvious that the modeling case being discussed (and the agreement of experiment with Monte Carlo calculations) for the H–C-foil system is not an isolated instance, and agreement can also be obtained for other combinations of beam and target.

It appears that this is the path to solving the inverse problem of reconstructing the elementary characteristics of atomic collision processes in the target material that are responsible for the multi-electron secondary emission phenomenon. This path will lead to a fruitful synthesis of the advances in the physics of atomic collisions and studies of secondary electron emission and eventually to a quantitative theory of the phenomenon.

5. CONCLUSION

In recent years, as seen from the foregoing discussion, new experimental methods for differential measurements of the characteristics of multiply emitted electrons have undergone vigorous development. Reliable new data have been obtained on the statistics and the energy and angular distri-

butions of secondary electrons, making it possible to test available models and to develop new theoretical models for the phenomenon. Through the interaction of this new information with theoretical approaches a way will be found to develop an adequate quantitative theory. In experimental studies of secondary electron emission the following seem to be the most interesting directions of development:

a) studies of thin metal targets;

b) the use of targets of different thickness for a controllable turn-on of various collision processes and a control of the charge state of particles passing through the target;

c) measurement of all the key parameters of multi-electron secondary emission in a single experiment;

d) measurements of the energy spectra of low-energy electrons (both reflected and transmitted) ($E_e < 20$ eV), which make the major contribution to the secondary electron yield;

e) the use of beams of multiply charged ions in the experiments and an investigation of isotopic effects for H and D beams.

[1] M. F. Villard, J. Phys. (Paris) **8**, 1 (1889).
[2] I. M. Bronshtein and B. S. Fraĭman, *Secondary Electron Emission* [in Russian], Nauka, Moscow (1969).
[3] V. P. Kovalev, *Secondary Electrons* [in Russian], Energoatomizdat, Moscow, 1987.
[4] G. Lakits, F. Aumayr, and H. Winter, Radiat. Eff. **109**, 129 (1989).
[5] K. S. Golovanivskiĭ and V. D. Dugar-Zhabon, Prib. Tekh. Eksp. No. 3, 7 (1991).
[6] H. Winter, Private communication (1990).
[7] G. Lakits, Dissertation, Techn. University of Vienna, 1989.
[8] W.-Q. Cheng, M. E. Rudd, and Y.-Y. Hsu, Phys. Rev. A **40**, 3599 (1989).
[9] Y. Yamazaki and K. Kuroki, Nucl. Instrum. Methods Phys. Res. A **262**, 118 (1987).
[10] H. Ritter, MPE Report 190, Garching, West Germany, 1985.
[11] K. Kuroki and Y. Yamazaki, Nucl. Instrum. Methods Phys. Res. B **33**, 276 (1988).
[12] G. Lakits, F. Aumayr, and H. Winter, Rev Sci. Instrum. **60**, 3151 (1989).
[13] M. A. Gruntman, A. A. Kozochkina, and V. B. Leonas, Prib. Tekh. Eksp. No. 3, 157 (1989) [Instrum. Exp. Tech. (USSR) **32**, 668 (1989)].
[14] B. Wilken, Rep. Prog. Phys. **47**, 767 (1985).
[15] M. Rubel *et al.*, Nucl. Instrum. Methods Phys. Res. B **47**, 202 (1990).
[16] A. A. Demchenkova, Prib. Tekh. Eksp. No. 5, 149 (1987) [Instrum. Exp. Tech. (USSR) **30**, 1182 (1987)].
[17] M. A. Gruntman and V. A. Morozov, J. Phys. E **15**, 1356 (1982).
[18] D. Hasselkamp, S. Hippler, and A. Scharmann, Nucl. Instrum. Methods Phys. Res. B **18**, 561 (1987).
[19] M. E. Rudd, Phys. Rev. A **38**, 6129 (1989).
[20] S. Suarez *et al.*, Nucl. Instrum. Methods Phys. Res. B **33**, 326 (1988).
[21] M. A. Gruntman, A. A. Kozochkina, V. B. Leonas, and M. Vitte, Izv. Akad. Nauk SSSR Ser. Fiz. **54**, 1377 (1990) [Bull. Acad. Sci. USSR Phys. Ser. **54**, No. 7 139 (1990)].
[22] A. A. Kozochkina, Preprint Pr-343 [in Russian], Institute of Problems in Mechanics, Academy of Sciences of the USSR, Moscow (1988).
[23] A. A. Kozochkina, G. A. Iferov, and V. Ya. Chumanov, *Proceedings of the 19th All-Union Conference on the Interaction of Charged Particles with Crystals*, State University, Moscow (1989), p. 78.
[24] H. Rothard *et al.*, Phys. Rev. A **41**, 2521 (1990).
[25] D. Hasselkamp, Comm. At. Mol. Phys. **21**, 241 (1988).
[26] A. Clouvas *et al.*, Phys. Rev. B **39**, 6316 (1989).
[27] G. Lakits, F. Aumayr, and H. Winter, Phys. Lett. A **139**, 395 (1989).
[28] D. A. Ralys and R. Kalytis, Bull. Vilnius Astron. Obs. No. 48, 3 (1978).
[29] D. Hasselkamp *et al.*, Z. Phys. D **6**, 269 (1987).
[30] D. Zajfman *et al.*, Phys. Rev. A **41**, 2482 (1990).
[31] R. J. Beuhler and L. Friedman, J. Appl. Phys. **48**, 3928 (1977).
[32] R. J. Beuhler, G. Friedlander, and L. Friedman, Phys. Rev. Lett. **63**, 1262 (1989).
[33] G. Lakits and H. Winter, Nucl. Instrum. Methods Phys. Res. B **48**, 597 (1990).
[34] J. Schou, Phys. Rev. B **22**, 2141 (1980).
[35] J. Schou, Scanning Micr. **2**, 607 (1988); **3**, 429 (1989).
[36] A. F. Akkerman and A. L. Gibrekhterman, Nucl. Instrum. Methods Phys. Res. B **6**, 496 (1985).
[37] D. M. Walker, Adv. Phys. **20**, 257 (1971).
[38] M. Gryzinski, Phys. Rev. **139**, 305 (1965).
[39] O. B. Firsov, Zh. Eksp. Teor. Fiz. **36**, 1517 (1959) [Sov. Phys. JETP **9**, 1076 (1959)].
[40] H. H. Fleischmann, R. C. Dehmel, and K. S. Lee, Phys. Rev. A **5**, 1784 (1972).
[41] B. E. Baklitskiĭ and E. S. Parilis, Zh. Tekh. Fiz. **56**, 27 (1986) [Sov. Phys. Tech. Phys. **31**, 15 (1986)].

Translated by Eugene R. Heath